





DIRECT GEOREFERENCING IN UNMANNED AERIAL VEHICLE USING QUASI-ZENITH SATELLITE SYSTEM

Agung SYETIAWAN¹, Yunus SUSILO^{2*}, Susilo SUSILO¹, Suroño SURONO³, Wahono WAHONO^{4,5}, Yudha Ahmad SIDDIQ⁶, Subekti HARTO⁷, Yustisi LUMBAN-GAOL¹, Abdurrahman ABDURRAHMAN⁵, Sutrisno SUTRISNO⁸ and Abdurrahman ABDURRAHMAN⁹

DOI: 10.21163/GT_2023.181.09

ABSTRACT:

To produce accurate topographic data, Unmanned Aerial Vehicle (UAV) still rely on Ground Control Points (GCPs) for georeferencing. However, using GCPs has several limitations, among others, related to the cost and time required for field measurements. In addition, not all areas are accessible for GCPs measurements due to poorly accessible terrain or security reasons. Direct georeferencing, a method to determine precise camera position and orientation in UAVs using Global Navigation Satellite System (GNSS) geodetic antenna. Post Processing Kinematic (PPK) or real-time coordinates can be applied to determine the camera position. One satellite that sends corrections to the rover on Earth is the Quasi-Zenith Satellite System (QZSS). This study aims to analyze the orthophoto accuracy of the results of direct georeferencing using precise coordinates from the QZSS satellites. The flight parameter was used at 60% sidelap and 80% overlap on an average flying altitude of 300 m above ground level resulting in 135 photos with a Ground Sampling Distance (GSD) value of 6 cm. The accuracy of direct georeferencing using QZSS horizontally and vertically was 1.134 m and 1.617 m, respectively. Meanwhile, the same metric results using conventional GCPs were 0.417 m horizontally and 0.419 m vertically. With these results, the horizontal accuracy of Direct Georeferencing using corrections from QZSS can be used for large-scale mapping of the 1: 5,000 class 1 scale, while vertical accuracy can be used for large-scale mapping of the 1: 5,000 class 3 scale. Direct georeferencing using QZSS corrections has the potential to support the acceleration of large-scale mapping activities in Indonesia.

Key-words: Direct Georeferencing, Unmanned Aerial Vehicle, Quasi-Zenith Satellite System, Large-scale mapping

¹Research Center for Geospatial, National Research and Innovation Agency (BRIN), Jakarta-Bogor Street Km. 46, Cibinong 16911, Indonesia, agungsyetiawan@gmail.com, susilosarimun@gmail.com, yust012@brin.go.id

²Geomatics Engineering, Dr. Soetomo University, Semolowaru 84 Surabaya 60111, Indonesia, yunus.susilo@unitomo.ac.id

³Magellan Systems Japan, Amagasaki Research Incubator Center, #315 7-1-3, Hyogo, Japan, surono@magellan.jp

⁴University of Muhammadiyah Malang, Tlogomas street No. 246, Malang 65145, Indonesia, wahono@umm.ac.id

⁵Moto Doro Teknologi, Bukit Cemara Tidar J4 No. 34 Sukun, Malang city, Indonesia, wahono@umm.ac.id, abdurrahman19940607@gmail.com

⁶PHW IV, Perhutani Divre Jawa Timur, Terusan Kawi No. 3, Malang, Indonesia, yudhaahmadsiddiq@gmail.com

⁷Licensed Cadastral Surveyor Service Office of Muchammad Masykur and partner, Kalila Residence C-10, Malang 65142, Indonesia, subekti_harto@yahoo.co.id

⁸Urban Navigasi Indonesia, Alam Bukit Raya resident C6 no 3, Randuagung, Gresik Regency, Indonesia, trisno.urbanav@gmail.com

⁹AMZ Geoinfo Solution, Gayungsari XI / 54, Surabaya, Indonesia, Abdurrahman9@gmail.com

*Corresponding author's email: yunus.susilo@unitomo.ac.id

1. INTRODUCTION

The use of Unmanned Aerial Vehicle (UAV) technology for mapping activities is escalating since it offers aerial photos with very high resolution. Compared to other methods such as satellite sensors, UAV-based photogrammetry provides more benefits regarding data acquisition and the resulting temporal resolution (Liu et al., 2022). With this capability, UAVs are often used for rapid mapping purposes such as disaster management (Restas, 2015), precision farming (Candiago et al., 2015;

Syetiawan & Haidar, 2019), landslides monitoring (Godone et al., 2020; D. Turner et al., 2015), and coastal changes (N Long et al., 2016; Nathalie Long et al., 2016).

The accuracy and precision of photogrammetry are highly dependent on various factors, including image quality, camera calibration, flight parameters, image processing algorithms, land cover and surface textures, and the intensity of sunlight (H. Zhang et al., 2019). To produce accurate topographic data, UAVs still rely on Ground Control Points (GCPs) for georeferencing (James et al., 2017; I. L. Turner et al., 2016). Meanwhile, the quality of GCPs depends on their density, which is the number and distribution (Sanz-Ablanedo et al., 2018). Georeferencing is the process of registering bundle adjustment results and photogrammetric processes to a particular coordinate system (Cramer et al., 2000; Kraus, 1993). However, using GCPs has several limitations, among others, related to the cost and time required for field measurements. In addition, not all areas are accessible for GCPs measurements due to poorly accessible terrain or security reasons, for example, swamp, glacier, or military areas.

Along with the development of current navigation satellite technologies, precise geodetic antennas can be integrated into UAV systems. The goal is that each aerial photo can be referenced at precise coordinates, a technique called direct georeferencing. The direct georeferencing process requires the device to have an accurate position up to cm-level to obtain a precise camera position and orientation in UAV measurements (Liu et al., 2022). Positioning computation methods, such as Post Processing Kinematic (PPK) or real-time coordinates where the corrections are obtained from radio signals or directly from satellites, can be applied to determine the camera position. One satellite that sends corrections to the rover on Earth is the Quasi-Zenith Satellite System (QZSS).

Some scholars have studied using QZSS for real-time kinematic positioning combined with multi-GNSS can improve positioning accuracy (Kitamura et al., 2014; Odolinski et al., 2015). QZSS is a regional augmentation satellite owned by Japan that is used as a complement to existing satellite systems like the Global Positioning System (GPS) or Beidou Satellite Navigation System (BDS) (Kubo et al., 2004; Wu et al., 2004). The QZSS satellite was first launched in 2010 and operated along with GPS and allows the combined processing of both systems (Hauschild et al., 2012). Furthermore, the raised number of QZSS satellites, becoming four in 2018, resulted in increased availability, reliability, integrity, and accuracy of positioning covering the Asia-Pacific region (Zaminpardaz et al., 2018; Q. Zhang et al., 2018). The QZSS satellites have three quasi-zenith orbits/QZO (QZS-1, QZS-2, QZS-4), but there is one satellite that has geostationary earth orbits/GEO (QZS-3) (Zhu et al., 2020). By 2023, QZSS is expected to be expanded to a seven-satellite system, which will enable it to provide better positioning, navigation, and timing (PNT) services (Li et al., 2021). It becomes an advantage for the direct georeferencing method in UAVs. This study aims to analyze the orthophoto accuracy of the results of direct georeferencing using precise coordinates from the QZSS satellites. The increased number of QZSS systems is expected to provide positive benefits, especially in rapid mapping applications using UAVs around Indonesia.

2. STUDY AREA

The aerial photo acquisition was carried out in Pandanlandung, Wagir sub-district, Malang Regency, Jawa Timur. The area of research is part of PERHUTANI, mainly dominated by vegetation, having an altitude of approximately 600 m above sea level and a total area of roughly 50 hectares. **Figure 1** illustrates the area of interest (AOI) in this study, where there are up to 100 m height differences between the eastern and western parts. Therefore, the aerial photos were captured at an average flying altitude of 300 m above ground level.

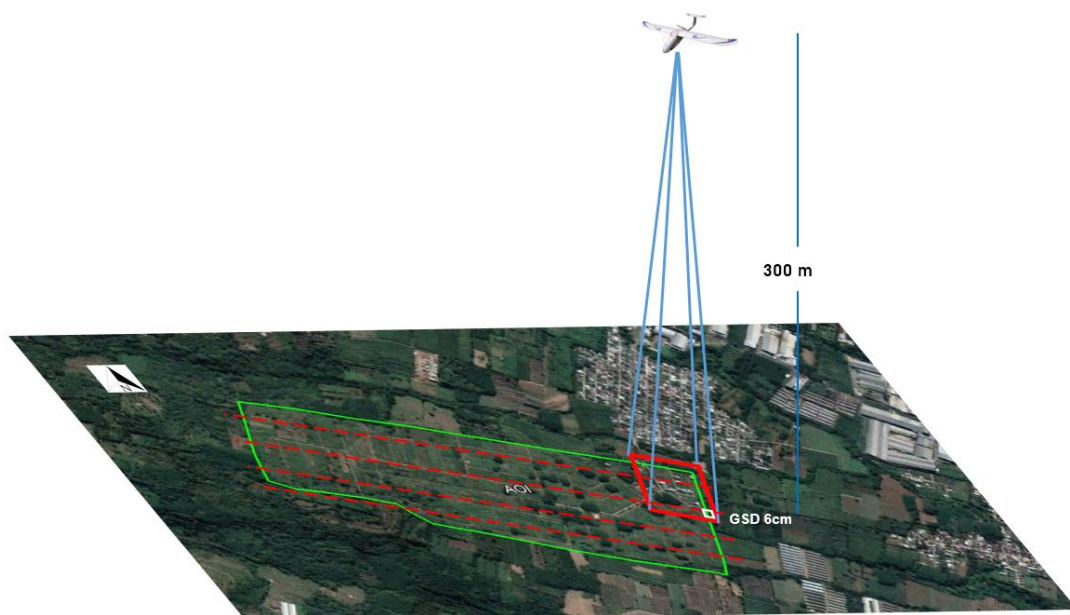


Fig. 1. Data acquisition parameters in the study area.

The flight was planned in the east-west direction with a Ground Sampling Distance (GSD) value of 6 cm. Subsequently, we used 60% sidelap and 80% overlap resulting in 135 photos with a flight duration of approximately 20 minutes.

3. DATA AND METHODS

3.1. Sensor and UAV specifications

For the aerial photo data collection, we used a fixed-wing UAV named FARM Mapper VTOL V2.0 2100 mm wingspan equipped with the Vertical Take-Off and Landing (VTOL) feature. Fixed-wing has the advantage of having more aerodynamic aircraft to fly longer than the multi-rotor type (Boon et al., 2017). **Table 1** (left) provides the complete specifications of the vehicle, and **Table 1** (right) depicts the specifications of the camera used. The UAV used a Sony A6000 type CMOS camera with a resolution of 24.3 Mega Pixels. This study used a mirrorless camera lens. Furthermore, the MSJ antenna was mounted on the top of the fixed-wing to receive the QZSS signal (can be seen in **Figure 2**). The offset between the MSJ antenna and non-metric camera was 13 cm vertically.



Fig. 2. QZSS antenna installation on Fixed-wing UAV.

Table 1.**UAV and Non-Metric Camera Specifications.**

FARM Mapper VTOL V2.0		Sony Alpha ILCE A6000	
Airframe:	Epo+Fibercarbon (Wingspan 2100mm)	Lens	E-mount Sony 20mm fixed, F2.8
Flight Controller:	Pixhawk cube orange	Pixel	24.3 MP
GPS Compass:	+ GPS here M8N	Sensor type	Sensor CMOS
Control System:	Manual and Auto	Dimension	120x67x45 mm
Radio Telemetry:	RFD 900x	Type	Mirrorless
Servo:	Emax 3504 MD	Sensor Optical	APS-C type (23.5 x 15.6 mm)
Motor:	4120 430 Kv*1 5008 400 Kv*4	Shutter speed	1/4000 to 30sec
Sensor:	Digital Airspeed sensor, Barometer, Magnetometer, 3 Axis Gyroscope	Processor	Bionz X image processor
Battery:	LiPo 16.000 MAh 6S (2unit)		

3.2. Control point parameter

This study compared orthophoto results from the direct georeferencing process using precise coordinates of QZSS and the conventional method using GCPs. Accordingly, we measured control points using geodetic GNSS and divided them into Ground Control Points (GCPs) and Independent Check Points (ICPs), as shown in **Figure 3**. There were 20 control points in total, of which eight points were GCPs, and the rest were ICPs. All control points were distributed evenly over the entire study area. The conventional orthophoto method uses GCPs for the georeferencing process and tests the accuracy of the results using ICPs. In contrast, the direct georeferencing method uses all control points to check the accuracy of the orthophoto result.

Control points were measured using a Leica GS14 and SOUTH Galaxy G1. The observation time of each point was one hour with an interval of five seconds for satellite recording data. The GNSS data processing was performed using the static differential method, which refers to a geodetic control point (ID: TTG.1290). This study used both satellite segments from GPS and GLONASS. **Table 2** presents complete GNSS data processing parameters to obtain the coordinates of each control point.

Table 2.**Control Point Processing Parameter.**

Parameter	Description
Positioning mode	Static differential
Base	TTG.1290
Frequencies signal	Dual Frequency (L1 and L2)
Datum	SRGI 2013 (ITRF.08 epoch 2012)
Elevation Mask (°)	10
Satellite data interval	5 seconds
Satellite ephemeris	Broadcast
Satellite segment	GPS and GLONASS

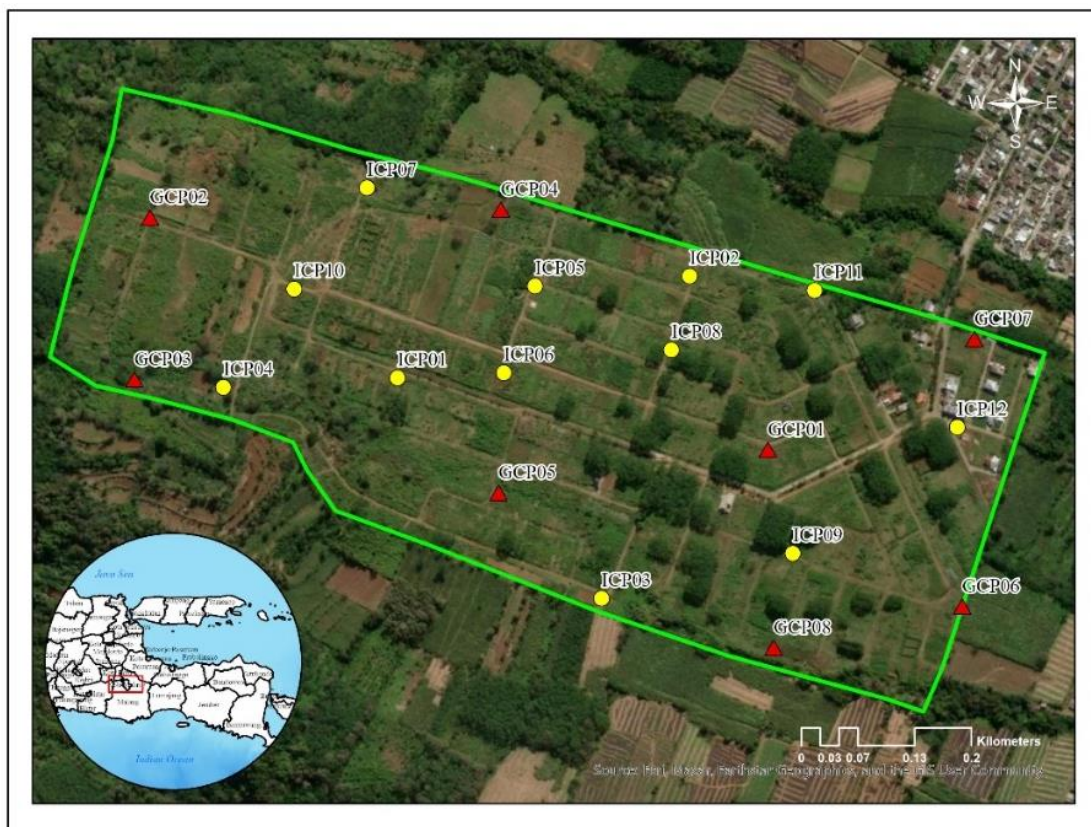


Fig. 3. Control points configuration in the study area. Red triangles represent GCPs, yellow circles are ICPs, and green lines represent areas of interest.

3.3. Accuracy assessment

This study assessed the accuracy of the orthophoto product from the direct georeferencing method and the use of GCPs by testing the geometric accuracy. The results were evaluated by comparing the coordinates of aerial photos with the control coordinates of the field measurements. The provisions for geometrical accuracy refer to the Regulation of the Head of the Geospatial Information Agency (BIG) No. 18 of 2021 regarding procedures for providing geospatial information. The geometric accuracy of the geospatial data is shown in **Table 3**. The geometric accuracy of the map is expressed in Circular Error with a confidence level of 90% (CE90) for the horizontal component and 90% Linear Error (LE90) for the vertical component. Measuring geometric accuracy was applied by calculating the Root Mean Square Error (RMSE) value. The RMSE values for the horizontal and vertical components can be seen in equations 1 and 2. Meanwhile, the calculation of the CE90 and LE90 values can be seen in equations 3 and 4, respectively:

$$RMSE_{horizontal} = \sqrt{\frac{\sum[(X_{data}-X_{check})^2+(Y_{data}-Y_{check})^2]}{n}} \tag{1}$$

$$RMSE_{vertical} = \sqrt{\frac{\sum[(Z_{data}-Z_{check})^2]}{n}} \tag{2}$$

$$CE90 = 1,5175 \times RMSE_{\text{horizontal}} \quad (3)$$

$$LE90 = 1,6499 \times RMSE_{\text{vertical}} \quad (4)$$

where n is the total number of checkpoints on the map, X is the coordinates on the axis – X , Y is the coordinates on the axis – Y , Z is the coordinates on the axis – Z , $RMSE_{\text{horizontal}}$ is the error at horizontal position (XY), and $RMSE_{\text{vertical}}$ the error at vertical position (Z). The horizontal position in this study refers to the UTM Projected Coordinate System, while the vertical position refers to the height of the WGS84 ellipsoid.

Table 3.
Geometry Accuracy of Geospatial Data Based on the Regulation of the Head of BIG No. 18 of 2021.

No	Aspect	1:5,000 scale			1:1,000 scale		
		Class 1	Class 2	Class 3	Class 1	Class 2	Class 3
1	Spatial resolution (m)	0.25	0.50	0.75	0.05	0.10	0.15
2	Hor. accuracy (CE90) (m)	1	2	3	0.20	0.40	0.60
3	Vert. accuracy (LE90) (m)	0.50	0.75	1	0.10	0.15	0.20

4. RESULTS AND DISCUSSIONS

Figure 4 shows the results of processing control points using commercial GNSS data processing software. The control point processing results show that the horizontal precision ranged from 0.007 m to 0.031 m, while the vertical precision ranged between 0.006 m and 0.098 m. Furthermore, the RMSE varied between 0.013 m and 0.039 m with the fixed solution of phase ambiguity for all control points. The accuracy results were sufficient for georeferencing or as a checkpoint.

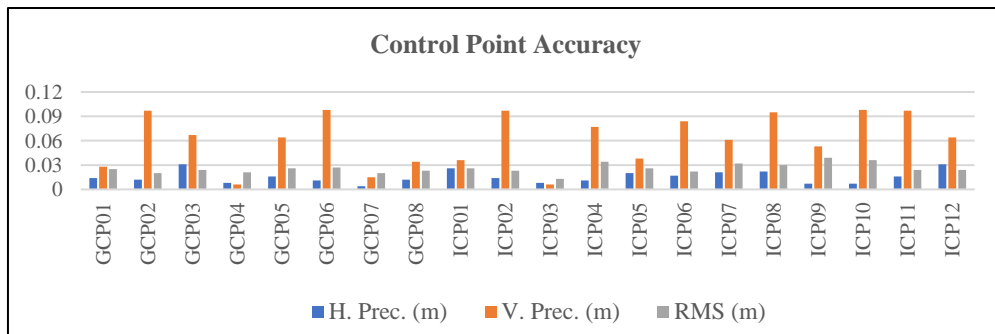


Fig. 4. Control point processing results.

The following process was to process aerial photos, where the geotagging process was first carried out to input QZSS precise coordinates into the photo. The precise coordinates of the QZSS satellite are used to determine the camera principal point position and external orientation parameters. **Figure 5** shows the reconstruction of aligned photos using accurate coordinates from the QZSS satellite. It shows that there is a misaligned photo, indicated by the small overlap area with the other photos. Furthermore, the tie point results of numerous pairs of overlapping photos are used to build dense point clouds (presented in **Figure 6**). The western part of the study area is densely covered with vegetations. In result, some places contain holes in the cloud due to imperfect tie point reconstruction. The total point cloud formed is 7,155,017 for the research area of 50 hectares.

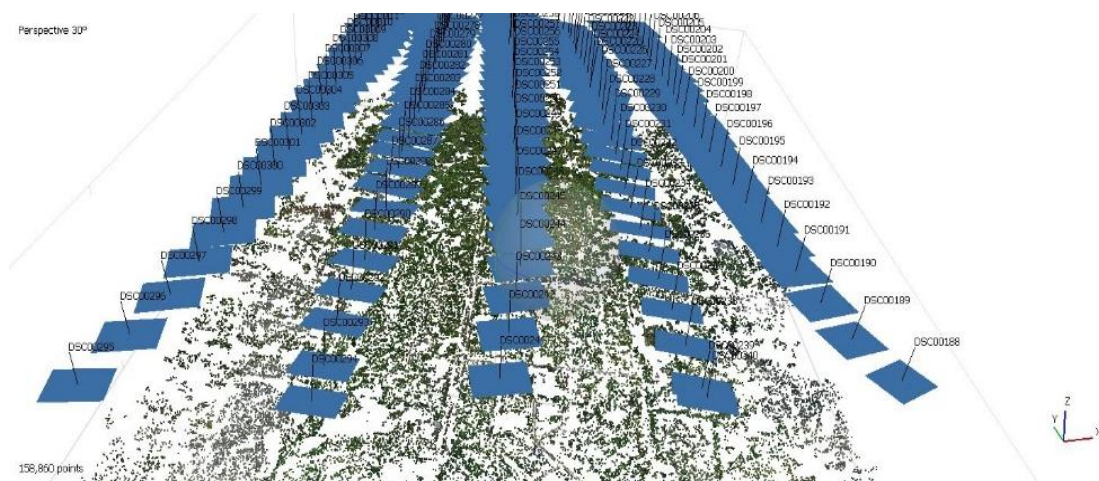


Fig. 5. Reconstruction of aligned photos using precise coordinates from the QZSS satellite.

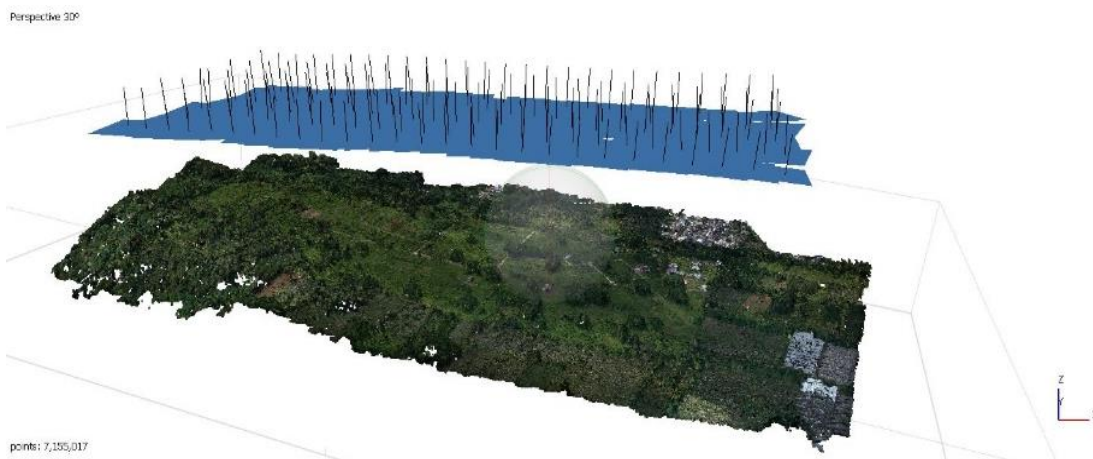


Fig. 6. Build dense cloud process.

The main difference between direct georeferencing using QZSS and conventional GCP is the process of obtaining accurate coordinates. Before acquiring aerial photo, QZSS receiver needs to initiate satellites for 5-10 minutes to fix coordinates. In contrast, conventional GCP requires a total observation time of around 8 hours (for 8 control points) according to the accuracy of the needed control points. Direct georeferencing based on Inertial Measurement Unit (IMU) and GNSS is preferred due to the time and cost efficiency than GCP field deployment, surveying, and recognition in images.

Figure 7 shows orthophoto mosaic results using direct georeferencing and conventional GCPs. The accuracy of direct georeferencing using QZSS horizontally and vertically was 1.134 m and 1.617 m, respectively (Table 4). Meanwhile, the same metric results using conventional GCPs (Table 5) were 0.417 m horizontally and 0.419 m vertically. A study by Turner et al. (Turner et al., 2012) showed similar results, where direct georeferencing yielded horizontal accuracy of 1.2 m when conventional GCPs increased the accuracy up to 0.10-0.15 m. The integration of QZSS and GPS can produce accurate Real-Time Kinematic Precise Point Positioning at an accuracy of up to cm level with 4-satellite constellation (Asari et al., 2016). However, in the application of moving vehicles, faster-fixed coordinates are needed. There is still error correction signal from QZSS due to satellite connection to fast-flying UAV and environmental characteristics around the measurement such as

ionospheric effect. Moreover, Syetiawan et al. (Syetiawan et al., 2020) revealed that direct georeferencing could produce a horizontal accuracy of up to 4 cm using post-processing kinematic in a relatively small research area. The direct georeferencing method relies heavily on the accuracy of the GNSS used to record the camera position. Instead of post-processed the camera position, the coordinates were directly corrected from QZSS in this study.

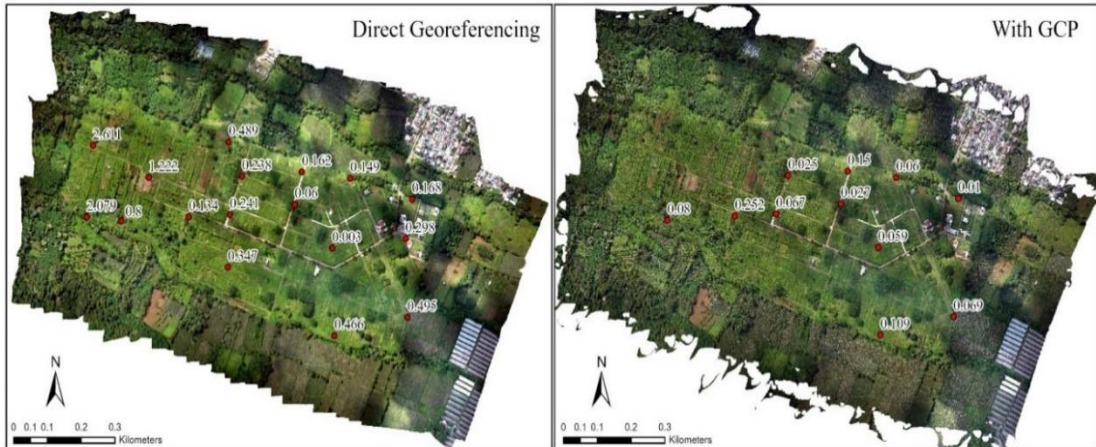


Fig. 7. Residue on horizontal components of direct georeferencing (left) and conventional GCPs (right).

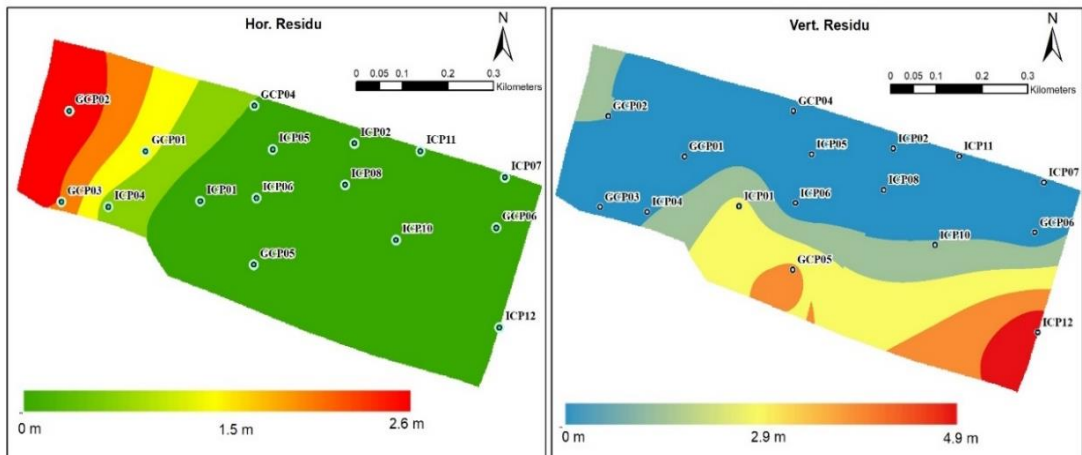


Fig. 8. Interpolation of residues of direct georeferencing method: Horizontal Residu (left); Vertical Residu (right).

The highest residue of the direct georeferencing result in the horizontal component was 2.6 m, while in the vertical component was 4.9 m. **Figure 7** illustrates the distribution of residue on the horizontal component, where GCPs-based mainly differ at the centimeter level, with the most considerable residue of 0.25 m at the ICP01 point. **Figure 8** shows the residual interpolation on the horizontal and vertical components using direct georeferencing. Overall, the most significant residue in horizontal occurred in the western part of the study area, which is steep, with an elevation difference of roughly 100 m compared to the east area.

In addition, direct georeferencing using QZSS corrections can be used for large-scale mapping of 1: 5,000 scale class 2 considering its horizontal accuracy and class 3 based on its vertical accuracy in **Table 3**. On the other hand, the horizontal and vertical accuracy of the conventional GCPs method

was suitable for large-scale mapping of 1: 1,000 scale class 3. Direct georeferencing using QZSS is less accurate than conventional GCP terms of accuracy. Direct georeferencing, however, is more effective at reducing field measurement time while ensuring accuracy. According to Sutanta et al. (2016), only a few areas have completed detailed mapping in Indonesia at scales of 1:5,000 and 1:10,000. Especially considering that Indonesia's land area is almost 2 million square kilometers. The need also increases along with the demand for topographic maps in detailed spatial plans. As a result, direct georeferencing with QZSS satellite correction has the potential to support the acceleration of large-scale mapping activities in Indonesia.

Table 4.

Horizontal and Vertical Accuracy of Direct Georeferencing.

ID point	Δx (m)	Δx^2	Δy (m)	Δy^2	Horizontal		Vertical
					in m (Δx^2 Δy^2)	+ Δz (m)	
GCP01	-0.058	0.003	-1.104	1.219	1.223	0.202	0.041
GCP02	-0.081	0.007	-1.614	2.605	2.612	-1.004	1.008
GCP03	0.359	0.129	-1.397	1.950	2.079	-0.701	0.491
GCP04	-0.500	0.250	-0.489	0.239	0.489	-0.717	0.514
GCP05	0.397	0.157	-0.436	0.190	0.347	1.776	3.154
GCP06	-0.157	0.025	0.523	0.274	0.298	0.594	0.353
ICP01	0.023	0.001	-0.365	0.133	0.134	1.524	2.323
ICP02	-0.233	0.054	-0.328	0.108	0.162	-0.543	0.295
ICP04	0.139	0.019	-0.884	0.782	0.801	0.940	0.884
ICP05	-0.105	0.011	-0.477	0.227	0.238	-0.279	0.078
ICP06	-0.090	0.008	-0.483	0.233	0.241	0.440	0.194
ICP07	-0.325	0.105	0.250	0.063	0.168	0.164	0.027
ICP08	0.095	0.009	-0.226	0.051	0.060	0.137	0.019
ICP10	0.038	0.001	0.043	0.002	0.003	1.046	1.094
ICP11	-0.361	0.131	0.135	0.018	0.149	-0.075	0.006
ICP12	0.230	0.053	0.665	0.442	0.495	2.213	4.897
Total					9.499		15.377
Variance					0.559		0.961
RMSE					0.748		0.980
Accuracy					1.134		1.617

Table 5.

Horizontal and Vertical Accuracy of Conventional GCPs.

ID point	Δx (m)	Δx^2	Δy (m)	Δy^2	Horizontal		Vertical
					in m (Δx^2 Δy^2)	+ Δz (m)	
ICP01	-0.049	0.002	0.500	0.250	0.252	-0.446	0.199
ICP02	-0.315	0.099	-0.224	0.050	0.150	0.150	0.022
ICP04	-0.026	0.001	0.282	0.080	0.080	-0.250	0.063
ICP05	-0.123	0.015	-0.101	0.010	0.025	0.236	0.056
ICP06	-0.256	0.066	0.030	0.001	0.067	0.418	0.175
ICP07	-0.074	0.005	-0.066	0.004	0.010	-0.173	0.030
ICP08	-0.130	0.017	-0.100	0.010	0.027	0.150	0.022
ICP09	-0.190	0.036	-0.270	0.073	0.109	-0.226	0.051
ICP10	-0.207	0.043	-0.128	0.016	0.059	0.084	0.007
ICP11	-0.244	0.060	0.011	0.000	0.060	-0.290	0.084
ICP12	0.042	0.002	-0.259	0.067	0.069	-0.024	0.001
Total					0.907		0.710
Variance					0.076		0.065
RMSE					0.275		0.254
Accuracy					0.417		0.419

5. CONCLUSIONS

The Direct Georeferencing method relies heavily on the accuracy of the GNSS used to record the camera position. The horizontal and vertical accuracy of the Direct Georeferencing method using QZSS was 1.134 m and 1.617 m. In accordance with BIG Head Regulation No. 18 of 2021, the horizontal and vertical accuracy is enough to create a large-scale map of 1: 5,000. The challenge ahead is to maintain the stability of the positioning satellite correction to obtain a precise position in real time. As a result, large-scale map creation can be completed quickly while retaining the quality of the final product.

This research still has a limitation because satellite coordinates recording does not coincide with the timing of the camera opening the lens. The UAV vehicle travels at a speed of 8-12 m/s, so it is not easy to synchronize the camera trigger with the sampling frequency of the GNSS receiver perfectly. Therefore, it is expected that there will be a fully integrated system in the future, where the GNSS antenna records the vehicle's position simultaneously with the camera records images.

ACKNOWLEDGMENT

This research was carried out following the Collaboration Agreement (Perjanjian Kerja Sama – PKS) No. 48/V/KS/07/2022 between the National Research and Innovation Agency Republic of Indonesia (BRIN) and the Faculty of Engineering UNITOMO. The authors would like to thank several parties for supporting this research. The study area and facilities used in this study were provided by Perhutani PHW IV Jawa Timur. Magellan System Japan (MSJ) provided the QZSS signal receiver device. Moto Doro and Urban Navigasi Indonesia supported the UAV equipment and the non-metric camera. The Licensed Cadastral Surveyor Service Office, Muchammad Masykur, equipped the GNSS device and carried out control point measurements. The natural disasters research program, Research Organization of Earth Sciences and Maritime, BRIN, partially financially supported this study with a grant number of B-676/III/PR.01.03/12/ 2021.

REFERENCES

- Asari, K., Matsuoka, S., & Amitani, H. (2016). QZSS RTK-PPP Application to Autonomous Cars. *Proceedings of the 29th International Technical Meeting of the Satellite Division of The Institute of Navigation (ION GNSS+ 2016)*, 2136–2142. <https://doi.org/10.33012/2016.14840>
- Boon, M. A., Drijfhout, A. P., & Tesfamichael, S. G. (2017). Comparison of a Fixed-Wing and Multi-Rotor Uav for Environmental Mapping Applications: a Case Study. *ISPRS - International Archives of the Photogrammetry, Remote Sensing and Spatial Information Sciences*, 47–54.
- Candiago, S., Remondino, F., De Giglio, M., Dubbini, M., & Gattelli, M. (2015). Evaluating Multispectral Images and Vegetation Indices for Precision Farming Applications from UAV Images. *Remote Sensing*, 7(4), 4026–4047. <https://doi.org/10.3390/rs70404026>
- Cramer, M., Stallmann, D., & Haala, N. (2000). Direct Georeferencing using GPS/Inertial Exterior Orientations for Photogrammetric Applications. In T. Schenk & G. Vosselman (Eds.), *International Archives of Photogrammetry and Remote Sensing. Vol. XXXIII, Part B3* (pp. 198–205). Amsterdam.
- Godone, D., Allasia, P., Borrelli, L., & Gullà, G. (2020). UAV and Structure from Motion Approach to Monitor the Maierato Landslide Evolution. *Remote Sensing*, Vol. 12. <https://doi.org/10.3390/rs12061039>
- Hauschild, A., Steigenberger, P., & Rodriguez-Solano, C. (2012). Signal, orbit and attitude analysis of Japan's first QZSS satellite Michibiki. *GPS Solutions*, 16(1), 127–133. <https://doi.org/10.1007/s10291-011-0245-5>
- James, M. R., Robson, S., & Smith, M. W. (2017). 3-D uncertainty-based topographic change detection with structure-from-motion photogrammetry: precision maps for ground control and directly georeferenced surveys. *Earth Surface Processes and Landforms*, 42(12), 1769–1788. <https://doi.org/10.1002/esp.4125>

- Kitamura, M., Ota, T., & Amano, Y. (2014). Improving Availability and Accuracy of Multi-GNSS Positioning Using QZSS. *Proceedings of the 27th International Technical Meeting of the Satellite Division of The Institute of Navigation (ION GNSS+ 2014)*, 2341–2345. Tampa.
- Kraus, K. (1993). *Photogrammetry*. Retrieved from <https://books.google.co.id/books?id=dJIQAQAIAAJ>
- Kubo, N., Wu, F., & Yasuda, A. (2004). Integral GPS and QZSS Ambiguity Resolution. *TRANSACTIONS OF THE JAPAN SOCIETY FOR AERONAUTICAL AND SPACE SCIENCES*, 47(155), 38–43. <https://doi.org/10.2322/tjsass.47.38>
- Li, X., Pan, L., & Yu, W. (2021). Assessment and Analysis of the Four-Satellite QZSS Precise Point Positioning and the Integrated Data Processing With GPS. *IEEE Access*, 9, 116376–116394. <https://doi.org/10.1109/ACCESS.2021.3106050>
- Liu, X., Lian, X., Yang, W., Wang, F., Han, Y., & Zhang, Y. (2022). Accuracy Assessment of a UAV Direct Georeferencing Method and Impact of the Configuration of Ground Control Points. *Drones*, Vol. 6. <https://doi.org/10.3390/drones6020030>
- Long, N., Millescamps, B., Pouget, F., Dumon, A., Lachaussee, N., & Bertin, X. (2016). Accuracy Assessment of Coastal Topography Derived from UAV Images. *The International Archives of the Photogrammetry, Remote Sensing and Spatial Information Sciences, XLI-B1*, 1127–1134. <https://doi.org/10.5194/isprs-archives-XLI-B1-1127-2016>
- Long, Nathalie, Millescamps, B., Guillot, B., Pouget, F., & Bertin, X. (2016). Monitoring the Topography of a Dynamic Tidal Inlet Using UAV Imagery. *Remote Sensing*, Vol. 8. <https://doi.org/10.3390/rs8050387>
- Odolinski, R., Teunissen, P. J. G., & Odiijk, D. (2015). Combined BDS, Galileo, QZSS and GPS single-frequency RTK. *GPS Solutions*, 19(1), 151–163. <https://doi.org/10.1007/s10291-014-0376-6>
- Restas, A. (2015). Drone Applications for Supporting Disaster Management. *World Journal of Engineering and Technology*, 03, 316–321. <https://doi.org/10.4236/wjet.2015.33C047>
- Sanz-Ablanedo, E., Chandler, J. H., Rodríguez-Pérez, J. R., & Ordóñez, C. (2018). Accuracy of Unmanned Aerial Vehicle (UAV) and SfM Photogrammetry Survey as a Function of the Number and Location of Ground Control Points Used. *Remote Sensing*, Vol. 10. <https://doi.org/10.3390/rs10101606>
- Sutanta, H., Aditya, T., & Astrini, R. (2016). Smart City and Geospatial Information Availability, Current Status in Indonesian Cities. *Procedia - Social and Behavioral Sciences*, 227, 265–269. <https://doi.org/10.1016/j.sbspro.2016.06.070>
- Syetiawan, A., Gularso, H., Kusnadi, G. I., & Pramudita, G. N. (2020). Precise Topographic Mapping Using Direct Georeferencing in UAV. *IOP Conf. Series: Earth and Environmental Science*, 1–10.
- Syetiawan, A., & Haidar, M. (2019). Pemetaan Perkebunan Sawit Rakyat dari Foto Udara Non Metrik Menggunakan Analisis Berbasis Objek. *Majalah Ilmiah Globè*, 21(1), 53–62. <https://doi.org/10.24895/MIG.2019.21-1.990>
- Turner, D., Lucieer, A., & De Jong, S. M. (2015). Time Series Analysis of Landslide Dynamics Using an Unmanned Aerial Vehicle (UAV). *Remote Sensing*, Vol. 7. <https://doi.org/10.3390/rs70201736>
- Turner, D., Lucieer, A., & Watson, C. (2012). An Automated Technique for Generating Georectified Mosaics from Ultra-High Resolution Unmanned Aerial Vehicle (UAV) Imagery, Based on Structure from Motion (SfM) Point Clouds. *Remote Sensing*, Vol. 4. <https://doi.org/10.3390/rs4051392>
- Turner, I. L., Harley, M. D., & Drummond, C. D. (2016). UAVs for coastal surveying. *Coastal Engineering*, 114, 19–24. <https://doi.org/10.1016/j.coastaleng.2016.03.011>
- Wu, F., Kubo, N., & Yasuda, A. (2004). Performance analysis of GPS augmentation using Japanese Quasi-Zenith Satellite System. *Earth, Planets and Space*, 56(1), 25–37. <https://doi.org/10.1186/BF03352488>
- Zaminpardaz, S., Wang, K., & Teunissen, P. J. G. (2018). Australia-first high-precision positioning results with new Japanese QZSS regional satellite system. *GPS Solutions*, 22(4), 101. <https://doi.org/10.1007/s10291-018-0763-5>
- Zhang, H., Aldana-Jague, E., Clapuyt, F., Wilken, F., Vanacker, V., & Van Oost, K. (2019). Evaluating the potential of post-processing kinematic (PPK) georeferencing for UAV-based structure-from-motion (SfM) photogrammetry and surface change detection. *Earth Surface Dynamics*, 7(3), 807–827. <https://doi.org/10.5194/esurf-7-807-2019>
- Zhang, Q., Yang, W., Zhang, S., & Yao, L. (2018). Performance Evaluation of QZSS Augmenting GPS and BDS Single-Frequency Single-Epoch Positioning with Actual Data in Asia-Pacific Region. *ISPRS International Journal of Geo-Information*, 7(5). <https://doi.org/10.3390/ijgi7050186>
- Zhu, S., Yue, D., He, L., Liu, Z., & Chen, J. (2020). Comprehensive analysis of compatibility between QZSS and GPS in Asia-Pacific region: Signal quality, RTK and PPP. *Advances in Space Research*, 66(2), 395–411. <https://doi.org/10.1016/j.asr.2020.04.003>